Research Square

Preprints are preliminary reports that have not undergone peer review.
They should not be considered conclusive, used to inform clinical practice,
or referenced by the media as validated information.

Influence of Sintering Temperature on the Structural, Microstructural, Dielectric and Electrical Properties of Ba 0.8Sr 0.2TiO 3 Ceramics

Jakkula Shankar
Geethanjali College of Engineering and Technology
Panthagani Raju
panthaganiraju@gmail.com
Geethanjali College of Engineering and Technology
Ale Shiva Kumar
Geethanjali College of Engineering and Technology
SK Mahammad Ali
Geethanjali College of Engineering and Technology
M. Sreelatha
MVSR Engineering College

Research Article

Keywords: Ba0.8Sr0.2TiO3 (BST), Solid-state reaction, Rietveld refinement, Grain-size analysis, Dielectric properties, Impedance spectroscopy

Posted Date: November 25th, 2026

DOI: https://doi.org/10.21203/rs.3.rs-11739001/v1

License: This work is licensed under a Creative Commons Attribution 4.0 International License.
Read Full License

Additional Declarations: No competing interests reported.

Influence of Sintering Temperature on the Structural, Microstructural, Dielectric and Electrical Properties of $Ba_{0.8}Sr_{0.2}TiO_3$ Ceramics

Jakkula Shankar[1], Panthagani Raju[1*], Ale Shiva Kumar[1], SK Mahammad Ali[1] and M. Sreelatha[2]

[1]Department of Physics, Geethanjali College of Engineering and Technology, Cheeryal, Kesara, Medchal, Telangana, India-501301.

[2]MVSR Engineering College, Nadergul Hyderabad Telangana India-501510

[*]Corresponding author email: panthaganiraju@gmail.com

Abstract

$Ba_{0.8}Sr_{0.2}TiO_3$ (BST) ceramics were prepared using solid-state method and sintered at 1100-1300 °C for 3 h. The effect of sintering temperature on Structural, microstructure, dielectric, and electrical properties were investigated using X-ray diffraction (XRD), Rietveld refinement, Williamson-Hall analysis, FESEM, dielectric spectroscopy, and impedance measurements. XRD confirmed perovskite structure without detectable secondary crystalline phases. The principal diffraction peak FWHM decreased from 0.298º to 0.104º, while FESEM revealed grain growth from 0.43 to 4.15 μm. Dielectric measurement showed temperature dependent changes in dielectric constant and dielectric loss, with the dielectric maximum occurring at 80 ºC. Modified Curie -Weiss analysis yielded a diffuseness exponent of 1.41 for BST1300, suggesting a diffuse dielectric transition. Impedance spectroscopy revealed non-ideal electrical relaxation, represented by a resistor-constant phase element equivalent circuit. Frequency dependent AC conductivity further demonstrated the influence of sintering induced microstructural evolution on electrical transport in BST ceramics.

Keywords: $Ba_{0.8}Sr_{0.2}TiO_3$ (BST); Solid-state reaction; Rietveld refinement; Grain-size analysis; Dielectric properties; Impedance spectroscopy.

1. Introduction

The perovskite ABO_3 structured lead-based ferroelectric ceramics have been investigatedwidely because of their outstanding properties such as dielectric, ferroelectric, piezoelectric, and pyroelectric properties; these properties are being utilized in electronic and energy storage applications. $BaTiO_3$ (BT) is most widely studied material owing to its excellent dielectric permittivity, relatively low loss, environmentally friendly properties, and excellent temperature-dependent polarization properties. Barium titanate based ceramics have found numerous applications including multilayer ceramic capacitors, thermistors, electro-optic devices, infrared detectors, sensors, actuators, and energy-storage capacitors [1-3]. The relatively high Curie temperature (~120°C), the comparatively weak temperature dependence of dielectric permittivity, and comparatively low dielectric tunability of pure $BaTiO_3$, however, restrict its performance for advanced tunable electronic and microwave applications. This has led to compositional

modification by isovalent substitution being an effective approach to modifying its crystal structure and functional properties.

BST ceramics are thus important dielectric materials for multilayer ceramic capacitors (MLCCs), voltage-controlled capacitors (varactors), tunable microwave filters, dielectric resonators, phase shifters, phased-array antennas, RF MEMS devices, microwave oscillators, energy storage capacitors and electro-optic modulators [4-5]. In particular, compositions that include between 15 mol% and 30 mol% Sr have a combination of high dielectric permittivity, moderate Curie temperature, low dielectric loss and tunability close to room temperature, which makes it suitable for next-generation wireless communication systems in the microwave and millimeter-wave frequency range [6]. Processing conditions such as sintering temperature also have a remarkable role on electrical and ferroelectric properties of BST ceramics. In solid-state sintering, the temperature decides the atomic diffusion, densification, grain-boundary migration, crystallite coarsening and defect annihilation. These all affect the final grain size [7], residual porosity, degree of crystallographic ordering, and concentration of oxygen vacancies and hence affect the dielectric polarization, domain-wall mobility, and electrical losses. Hence, it is important to optimize the sintering temperature to get dense BST ceramics with good dielectric properties.

J. Shankar et al [8] have investigated $Ba_{1-x}Sr_xTiO_3$ ceramics and found that increase in sintering temperature from 1000 ºC to 1200 ºC caused in rise in grain size and density and also found that the BST ceramics exhibit the relaxor-type characteristics. Jan Suchanicz et al [9] have also examined role of temperature on physical and dielectrical properties of $Ba_{1-x}Sr_xTiO_3$ ceramics, and found that the addition of Sr^{2+} ions into barium titanate led to a tetragonal to cubic phase transition temperature shift to lower temperatures with rise in content of strontium doping. They have also reported that the ferroelectric properties were decreased with a rise in the Sr doping. A few research studies [10-11] have been conducted to find the composition-related effect on phase transition and electrical properties of barium strontium titanate ceramics. Shiva Kumar et al. [12] were investigated $Ba_{0.9}Sr_{0.1}TiO_3$ ceramics and found that the increase in the sintering temperature from 1000 ºC to 1200 ºC, grain size and density increased and the sample heat treated at 1200 ºC for 3 hours showed minimum porosity. R. E. Patru et al. [13] have investigated the role of grain size on physical, phase transitions, electrical and ferroelectric properties of BST ceramics and found that with the rise in grain size, the tetragonality increased and peak dielectric constant increased from a few hundred to few thousands. And also observed that Curie-Weiss temperature, Curie constant decreased with the decrease in the grain size of BST ceramics indicating decrease in ferroelectric nature. J. Cirkovic et al. [14] have investigated the sintering temperature role on structural parameters, phase composition, electrical properties of BST ceramics and found that the major crystalline phase was the tetragonal BST and the BST ceramic sintered at 1280 ºC for 16 hours exhibited the highest density (93%,) and maximum ε_m (2300) and remnant polarization P_r (2 $\mu C/cm^2$).

Although the effect of sintering temperature on $Ba_{1-x}Sr_xTiO_3$ ceramics has been investigated extensively, the relationship between sintering induced microstructural evolution and separate grain

and grain boundary contributions to dielectric and electrical transport remains insufficiently resolved for $Ba_{0.8}Sr_{0.2}TiO_3$ ceramics synthesized by the solid state route. In particular, the evolution of crystallite size and microstrain, grain growth and densification, dielectric relaxation, impedance response and frequency dependent charge transport should be considered together to establish a quantitative processing micro-structure electrical property relationship. The authors previously investigated the physical and microstructural evolution of $Ba_{1-x}Sr_xTiO_3$ ceramics under different heat treatment conditions [8]. The present study is deliberately differentiated from that work by focusing on the electrical response of $Ba_{0.8}Sr_{0.2}TiO_3$ composition and, in particular, on the relationship between sintering induced microstructural development and dielectric relaxation. In the present work, impedance spectroscopy and ac conductivity measurements are integrated with crystallographic and microstructural characterization to examine the contributions of grains and grain boundaries to the overall electrical response. Thus, the objective is not merely to reproduce the previously reported structural and microstructural evolution, but to establish how these changes influence dielectric relaxation and charge transport.

The present study focuses specifically on $Ba_{0.8}Sr_{0.2}TiO_3$ ceramics sintered at 1100, 1150,1200,1250 and 1300 ^oC for 3 hours. The objective of present work is to examine how sintering temperature affects the structural parameters, diffraction broadening, grain size distribution, dielectric response, dielectric phase transition behavior, impedance spectra, and AC conductivity. By correlating these results, the study seeks to establish a processing-microstructure-property relationship for BST ceramics while distinguishing directly measured trends from interpretations of underlying electrical mechanisms.

2. Experimental Procedure

The preparation of polycrystalline BST ceramics was carried out by solid-state method using high purity analytical grade precursor powders of $BaCO_3$ (>99.9%, Sigma-Aldrich), $SrCO_3$ (>99.9%, Sigma-Aldrich) and TiO_2 (anatase form, >99.9%, Sigma-Aldrich). The initial powders were weighed based on the stoichiometric ratio of the composition of barium carbonate, strontium carbonate, and TiO_2 on an electronic balance with a precision of ±0.1 mg. A Retsch PM100 planetary ball mill was used to thoroughly mix the weighed powders. To prevent contamination, ethanol was used as the milling medium, and zirconia milling jars and zirconia balls were used for milling. The milling process was repeated for 20 h at a constant rotation speed to achieve homogeneous mixing and to obtain a smaller particle size. The slurry obtained after milling is heated in an oven at 100 °C till complete evaporation of ethanol. The dried powder was crushed in an agate mortar and pestle to make a fine, consistent powder. The mixed powder was then heated at 900 °C for 4 h in ambient air to facilitate the solid-state reaction and the formation of BST perovskite phase. The powder was subjected to calcination and then crushed and sieved to remove soft agglomerates. The total amount of polyvinyl alcohol (PVA) added was about 2 wt. % to enhance green strength of compacted pellets. Powders were uniaxially pressed into the pellets of 10 mm dia and 2 mm thick at 4 tons of pressure in a hydraulic press. Green pellets were subsequently sintered in air at different temperatures of 1100 °C, 1150 °C, 1200 °C,1250 °C, 1300 °C for 3 h using an

electrically heated programmable muffle furnace. Heating and cooling rates were kept at 5 °C per minute to avoid any thermal stresses and cracking during sintering. XRD was used to probe the phase change and crystal structure of sintered BST ceramics. At room temperature, diffraction patterns were taken on a diffractometer with Cu Kα radiation (λ = 1.5406 Å), 40 kV, 30 mA. The diffraction data was collected in a 2θ range of 10 -70° with a step size of 0.02° and speed of 2° min^{-1}. These diffraction patterns were analyzed with the Rietveld refinement technique with FULLPROF suite in order to determine the Bragg R-factor, RF-factor, and goodness-of-fit (χ^2). ApreoS make FESEM was utilized to examine microstructure of the sintered ceramics. PSM 1700 impedance analyzer from Newton's 4th Ltd was employed to study electrical properties.

3.Results and Discussion

Figure 1 depicts XRD pattern of BST ceramic heat treated at various temperatures from 1100 ^oC to 1300 ^oC for 3 hours. All major diffraction peaks can be indexed as (110) (111) (200) (210) (220) of perovskite tetragonal phase with P4mm space group on the XRD pattern with standard JCPDS No 00-044-0093. A similar result was observed for the BST ceramics by S. Yousuf and M. Ikram [15]. It was also found that no other secondary phases were observed and all XRD peaks were successfully indexed to single-phase perovskite structure of BST, indicating the successful formation of desired composition following the solid-state route. This observation further suggests that Sr^{2+} ions are incorporated into the $BaTiO_3$ lattice successfully to yield a homogeneous BST solid solution. From Table1 it is clearly evident that strongest diffraction peak, around 2θ ≈ 33°, is almost constant over the whole temperature range investigated, which means that the perovskite framework is structurally stable during sintering. The minor difference in the position of the peak in XRD (Table 1) corresponds to small changes in lattice spacing may be attributed to the thermal relaxation of internal stress and is not corresponds to any structural phase transition. It is also found from Table 1 that full width at half maximum (FWHM) values decreases progressively as sintering temperature increases from 0.298° for sintered sample at 1100 °C to 0.104° for sample sintered at 1300 °C, which corresponds to about 65% reduction in peak broadening. Because diffraction broadening may arise from both finite crystallite size and lattice microstrain, this change should not be attributed to crystallite growth without considering the instrumental contribution and results of line broadening analysis. The same kind of narrowing diffraction peaks has also been reported by R.E. Patru et al. [13] for BST ceramics.

The d-spacing corresponding to the main diffraction peak of the X-rays changes slightly from 2.691 to 2.715 Å. The behaviour indicates that the changes in the crystallinity and microstructural development are mainly due to sintering temperature, and that the intrinsic crystal symmetry of BST is not affected. The experimental and calculated diffraction profiles obtained from Rietveld refinement are shown in Figure 2, and the corresponding refined parameters are summarised in Table 2. The refined lattice parameters remain within a relatively narrow range over the investigated sintering temperature interval, indicating that the average crystal structure is retained during sintering. The goodness of fit values (χ^2 = 2.26 to 3.85) indicates acceptable refinement quality. The Bragg R-factor decreases overall from 9.223 for BST1100 to 2.814 for

BST1300, with a small increase at 1250 ºC. The progressive reduction in diffraction broadening is consistent and improved structural coherence at higher sintering temperature [16]. The lattice parameters are almost constant, suggesting the thermodynamic stability of the crystal structure in the range of sintering temperatures studied. An important observation is the continuous drop in the Bragg R factor with rise in sintering temperature; BST sample that was sintered at 1300 °C showed the best crystallographic quality. The results show that the higher the sintering temperature, the more structural ordering will be achieved, but the intrinsic crystal structure of the material will not be significantly changed [17].

Scherrer equation (1) gives a good approximation of crystallite size but assumes broadening of the diffraction peaks is only because of the dimensional limitation of the crystallites.

$$D = \frac{k\lambda}{\beta \cos\theta} \qquad (1)$$

where D is size of crystallite, k is shape factor (0.9), λ = 1.5418Å, β is FWHM, and θ is Bragg angle. For practical ceramic systems, the broadening of the peak in addition includes contributions from lattice strain. Williamson–Hall (W–H) analysis was therefore used to isolate these two effects from each other using equation (2)

$$\beta \cos\theta = \frac{k\lambda}{D} + 4\varepsilon \sin\theta \qquad (2)$$

where **ε** represents the lattice strain determined from slope and crystallite size from Y-intercept of W-H plots are given in Figure 3(a-e). The Williamson–Hall results are given in Table 3. The William-Hall slopes remain within a narrow range over the investigated temperature interval, indicating that the residual microstrain are of the order of 10^{-4} is comparatively insensitive to sintering temperature. The estimated crystallite sizes are approximately 46-50 nm. The crystallite size estimates do not show a clear monotonic increase with sintering temperature. In contrast, the reduction in peak broadening and the corresponding changes in the intercept indicates that the crystallite coarsening is the dominant structural evolution. Difference between crystallite size and FESEM grain size are expected because an individual ceramic grain may contain multiple coherently diffracting domains. Similar findings have been reported by P. Saroha et al. for BST ceramics [18].

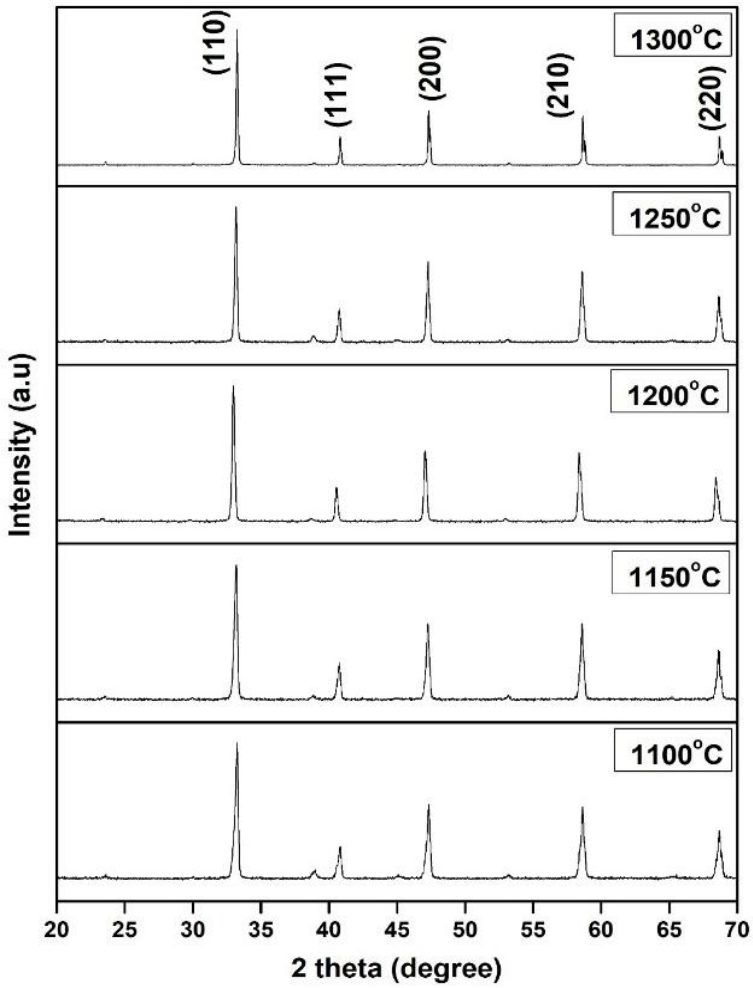

Figure 1. XRD patterns of $Ba_{0.8}Sr_{0.2}TiO_3$ ceramics sintered at different temperatures

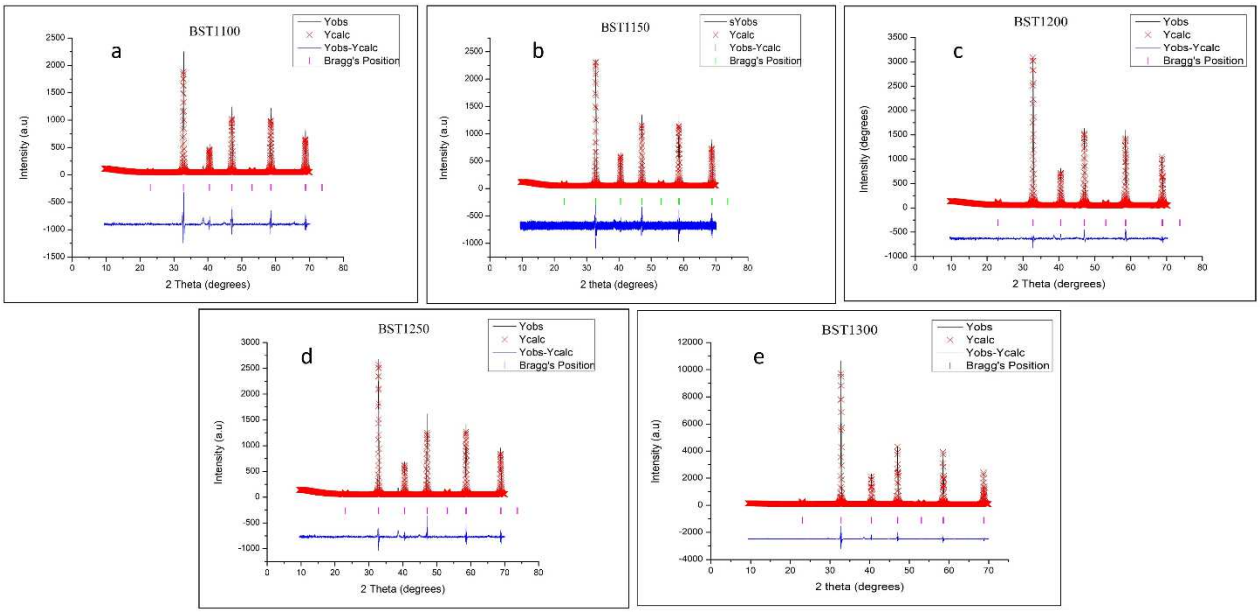

Figure 2(a-e). Rietveld refined XRD patterns of BST ceramics sintered at different temperatures

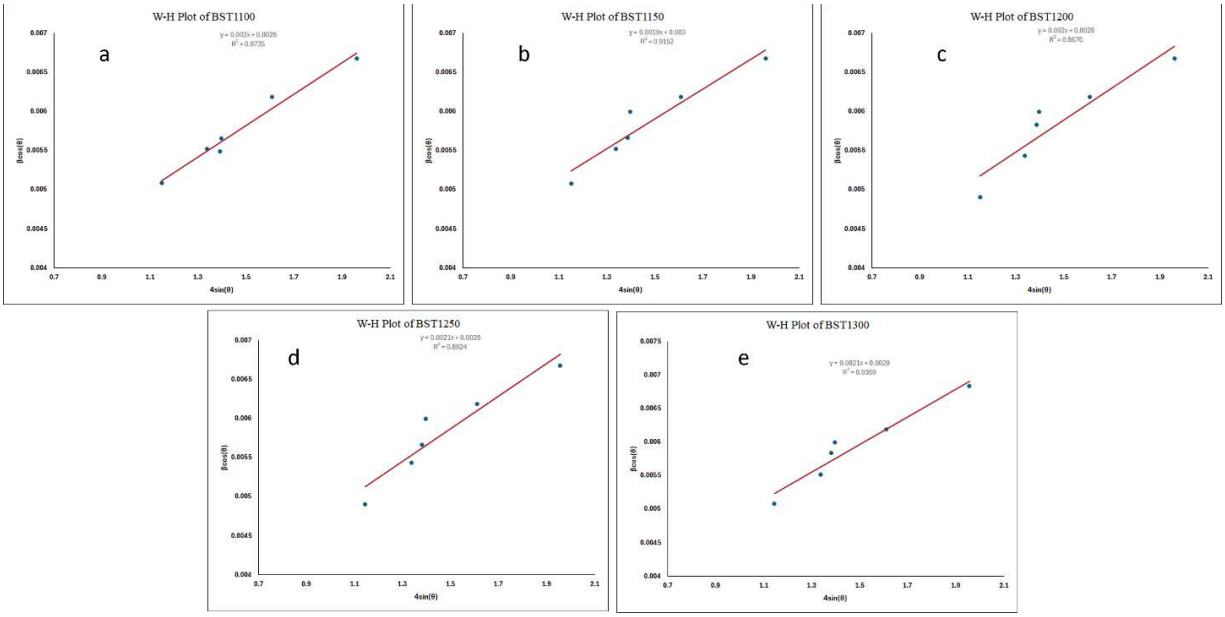

Figure 3(a-e). Williamson-Hall plots of BST ceramics sintered at different temperatures.

Table 1. Principal peak parameters extracted from the XRD patterns

Ceramic sample	Main peak 2θ (°)	d-spacing (Å)	FWHM (°)	Relative intensity (%)
BST1100	33.262	2.69136	0.298	100
BST1150	33.198	2.6964	0.249	100
BST1200	32.969	2.7146	0.209	100
BST1250	33.179	2.6979	0.187	100
BST1300	33.24	2.69304	0.104	100

Table2. Rietveld-refined parameters for $B_{0.8}S_{0.2}TiO_3$ ceramics

Ceramic Sample	**a(Å)**	**b(Å)**	**c(Å)**	**c/a**	**V = a^2c**	**χ^2**	**Bragg R-factor(%)**	**RF-factor(%)**
BST1100	3.860762	3.860762	3.899542	1.010045	58.1246	3.85	9.223	5.271
BST1150	3.85955	3.85955	3.897831	1.009919	58.0626	2.73	5.641	3.743
BST1200	3.859092	3.859092	3.897113	1.009852	58.0381	2.26	3.213	2.587
BST1250	3.858691	3.858691	3.886391	1.007179	57.8664	2.75	3.58	3.089
BST1300	3.861855	3.861855	3.87123	1.002428	57.7352	3.21	2.814	1.875

Table 3. Williamson–Hall crystallite size and lattice strain of $B_{0.8}S_{0.2}TiO_3$ ceramics heat-treated at different temperatures

Ceramic Sample	**Crystallite size (nm)**	**Lattice strain**
BST1100	49.56	$5.00x10^{-4}$
BST1150	46.25	$4.75x10^{-4}$
BST1200	49.56	$5.00.x10^{-4}$
BST1250	49.56	$5.25x10^{-4}$
BST1300	47.85	$5.25x10^{-4}$

The FESEM micrographs shown in Figure 4(a-e) show that the microstructures change greatly with rise in the sintering temperature. The ceramic is relatively fine-grained at 1100 °C with many interconnected pores between the grains. The irregular grain morphology suggests that the densification is still in the intermediate stage of solid-state sintering, with incomplete bonding of particles. Grain growth is restricted by the limited mobility of the grain boundary, which makes grain boundary structure porous. Grain-boundary diffusion increases significantly with sintering temperature of 1150 °C. Grains become more equiaxed, and the number of open pores is drastically reduced. Accelerated mass transport is suggested by an improvement in the growth of the neck between adjacent particles. Further heating to 1200 °C, results in the microstructure becomes denser and well-developed grain boundaries. As grain-boundary diffusion and lattice diffusion becomes more effective, the pore volume is greatly reduced. In the specimen sintered at 1250 °C, polygonal grains are seen with only a few pores at the triple-grain junctions. This microstructure is representative of the late stages of ceramic sintering, when the densification is roughly complete and grain growth is the predominant process. Microstructure of the sintered ceramic at 1300 °C is extremely dense, with uniformly distributed polygonal grains and with minimal porosity. Exaggerated grain growth is not observed, which means that the diffusion is homogeneous throughout the ceramic body. Such a dense microstructure is generally associated with a reduced contribution from residual porosity to the measured dielectric response. The FESEM observations clearly show that the grain-boundary mobility increases, pores are eliminated and dense ceramics are obtained with better structural homogeneity as the sintering temperature is increased. The FESEM micrographs were examined using imageJ software and the average grain size was measured for each specimen in order to quantitatively evaluate the microstructural evolution. Grain size rises systematically from 0.43 μm at 1100 °C to 1.38 μm at 1150 °C, 1.60 μm at 1200 °C, 3.17 μm at 1250 °C, and finally 4.15 μm at 1300 °C. Normal grain growth, by grain-boundary migration, is manifested by the gradual increase between 1100 and 1250 °C. By comparison, the very large increase at 1300 °C suggests that the grain-boundary mobility has increased significantly. Similar results [19-20] have been reported for BST ceramics, where the grains were dense, compact, and spherical in shape.

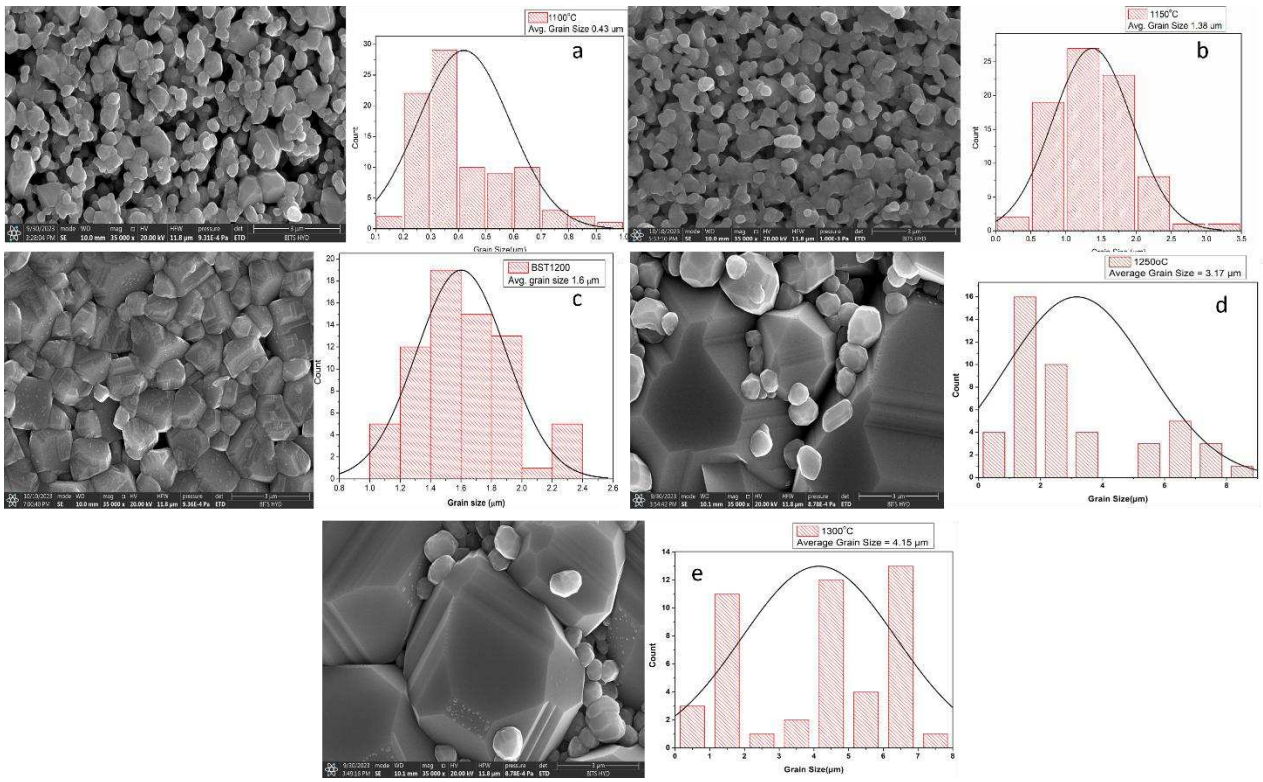

Figure 4 (a-e) FESEM micrographs and associated grain size images of BST ceramics

The room temperature dielectric permittivity and loss tangent of BST ceramics as a function of frequency are depicted in figures 5(a-b) respectively. It is observed that both dielectric constant and dielectric loss decrease rapidly with the rise in frequency. This dielectric dispersion may be attributed to Maxwell-Wagner interfacial polarization mechanism, indicating dielectric response of BST ceramics strongly depends on the grain and grain boundary microstructure developed during sintering. Temperature dependence of dielectric permittivity (ε_r) of BST ceramics heated at various temperatures at a frequency of 1 kHz is shown in Figure 6(a). All the BST ceramic samples sintered at various temperatures have the typical temperature dependence of dielectric constant of ferroelectric perovskite ceramics, in which dielectric constant rises gradually with temperature, peaks at the dielectric phase transition, and then falls in paraelectric phase. Dielectric maxima are related to the Curie temperature (Tc) of 80 ^{o}C at which the spontaneous polarization vanishes because of change from tetragonal ferroelectric phase to the cubic paraelectric phase. Dielectric constant gradually rises with the sintering temperature.

The result of increasing dielectric constant with sintering temperature may be ascribed to the improvement of densification and grain growth. As sintering temperature rises, grain-boundary diffusion increases, and it is possible to eliminate pores, and grain size rises from 0.43 µm to 4.15 µm. It is found that grain boundaries usually have a lower dielectric constant than grain interiors due to the presence of higher numbers of defects, trapped charges, and space-charge regions in the grain boundaries. The Curie temperature is nearly constant at around 80 ^{o}C for all BST ceramics

sintered at various temperatures, indicating that influence of sintering temperature is on microstructure and not the intrinsic crystal chemistry. The observed behavior is consistent with the reported studies [7, 21-22] on BST ceramics, which reported that dielectric properties were improved with increasing of sintering temperature because of an rise in density and grain size, in addition to the decrease in structural defects.

Figure 6(b) depicts dielectric loss (tan δ) variation with temperature. The dielectric loss rises slowly with temperature and has a wide peak around 80 ºC, the Curie temperature, as is the case with the dielectric constant. The behaviour is typical of ferroelectric ceramics, where the dielectric loss may be ascribed to several mechanisms such as dipolar relaxation, thermally activated charge transport, domain-wall motion, and space-charge polarization. BST ceramic sample which is sintered at 1100 °C, has maximum dielectric loss over the temperature range under study. This behavior is due to its porous microstructure and high amount of grain boundaries. Grain boundaries serve as trapping centres for the charge carriers, and interfacial polarization will be increased, which will lead to a rise in the dielectric loss. In addition, the electric field is concentrated locally at the remaining pores, leading to higher dielectric losses [23].

Dielectric loss is reduced gradually with rise of sintering temperature. At 1300 °C, BST ceramic sample has the lowest loss and the highest dielectric constant. It may be attributed to better densification, as it helps in suppressing the extrinsic loss mechanisms. The decrease in dielectric loss is found to be closely coupled with the structural evolution that is seen in FESEM images, showing a progressive decrease in porosity, improvement in crystallinity, and reduction in defect concentration. These improvements reduce the amount of charge trapping that occurs at grain boundaries and reduce leakage paths, resulting in a reduced amount of dielectric dissipation. It found that dielectric permittivity of BST ceramics increases and dielectric loss decreases with rise in sintering temperature, clearly reflecting that dielectric properties of BST ceramics are enhanced significantly by optimizing the microstructure.

The Curie temperature was found at point of maximum dielectric constant. Curie temperature of all the BST samples investigated is close to 80 ± 2 °C, which means that the ferroelectric–paraelectric phase transition is not significantly affectd by sintering temperature. A diffuse ferroelectric phase transition is indicated by the broad dielectric peaks, seen in all specimens, as opposed to a sharp transition temperature Tc. The diffuse behaviour is typical of $Ba_{1-x}Sr_xTiO_3$ solid solutions, where the distribution of local Curie temperatures is caused by random substitutions of Sr^{2+} ions in the structure.

At temperatures above the Curie temperature, the dielectric performance of BST ceramics is in accordance with the classical Curie–Weiss relation.

$$\frac{1}{\varepsilon r} = \frac{T - To}{C} \qquad (3)$$

C is Curie–Weiss constant, and T_0 is Curie–Weiss temperature.

Reciprocal dielectric constant depicts a nearly linear temperature dependence in the paraelectric phase, which is consistent with the Curie-Weiss dependence above Tc. Curie–Weiss constant is indicative of strength of the dipolar interactions in the perovskite lattice, while Curie–Weiss temperature is related to stability of the ferroelectric phase. The transition is not quite sharp and is observed to be linear with some slight deviations around Tc. This type of deviation comes from the random distribution of Ba^{2+} and Sr^{2+} ions over the A-site of perovskite structure. The ferroelectric phase transition in the BST ceramic, which was sintered at 1300 °C, was analysed with the modified Curie–Weiss relationship [24] to determine the degree of diffuseness of transition.

$$\left(\frac{1}{\varepsilon r} - \frac{1}{\varepsilon m}\right) = \frac{(T-Tm)^{\gamma}}{C} \quad (4)$$

where γ is the diffuseness exponent. εm is maximum dielectric constant and, Tm is peak temperature at which ε is maximum. If the material is an ideal ferroelectric, γ is close to unity, while γ is close to two for a relaxor ferroelectric. The modified Curie–Weiss analysis of the BST ceramic is shown in Figure 7 (a-b), which shows the diffuse phase transition model because the calculated γ is 1.41. Similar results have been reported in the literature [25-26].

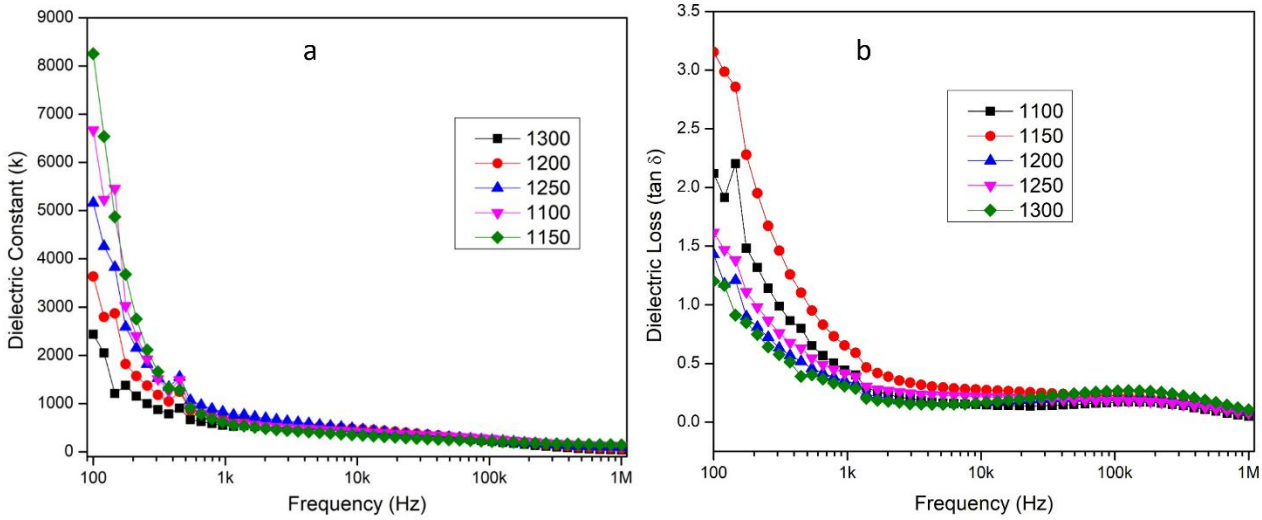

Figure 5(a) RT dielectric constant as a function of frequency for BST ceramics. (b) RT dielectric loss as a function of frequency for BST ceramics

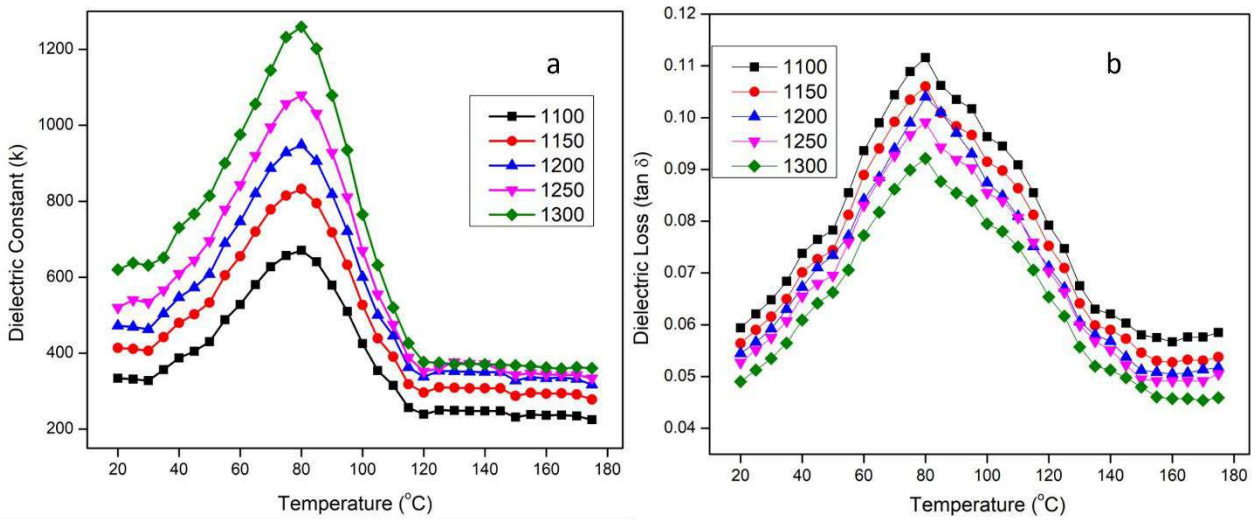

Figure 6(a) Variation of dielectric constant as a function of temperature for BST ceramics at 1 kHz. (b) Variation of dielectric loss as a function of temperature for BST ceramics at 1 kHz

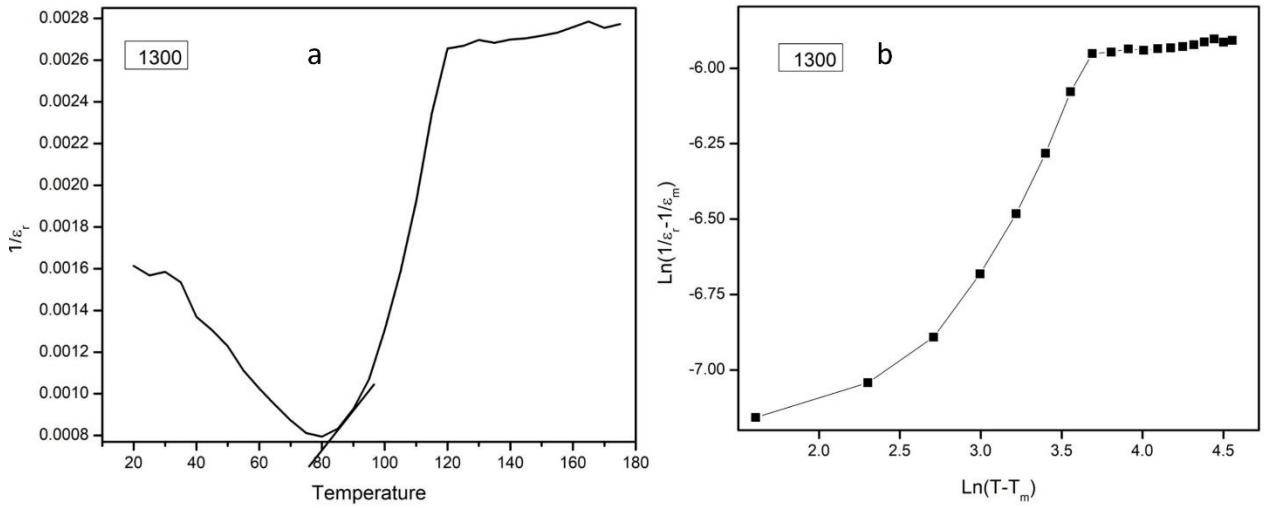

Figure 7(a) Reciprocal of dielectric constant with temperature for BST ceramic sintered at 1300 °C. (b) Fitting of modified Uchino Law for BST ceramic sintered at 1300 °C

Real part of impedance (Z') is shown in figure 8(a) for the BST ceramics. It is clearly seen that the Z' decreases with rise in frequency for all the sintered samples and reaches nearly zero at higher frequencies. The high values of Z' at lower frequencies denotes the resistive contributions of grain boundaries and electrode polarization. When the frequency rises, these polarization effects decrease and resulting the decrease of Z'. The lower Z' values observed for BST1300 sample indicates a reduction bulk resistance because of improved grain growth and densification, and decreased grain boundary density. Figure 8(b) depicts imaginary part of impedance (Z'') as function of frequency. BST ceramics sintered at various temperatures show a broad relaxation peak in the

low frequency region, and further increase in frequency resulted in the decrease of Z".This behaviour may be ascribed to the non-Debye type relaxation process, denotes the presence of distribution of relaxation times due to the structural heterogeneity, grain and grain boundary contribution. The variation in peak position with sintering temperature indicates the change in electrical resistance relaxation behaviour caused by microstructural development during the sintering.

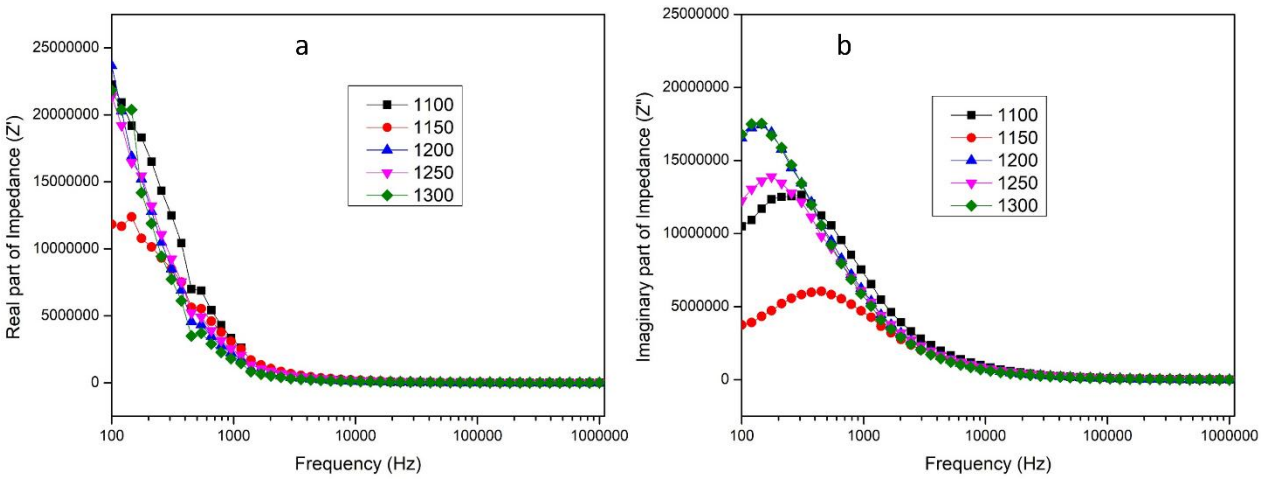

Figure 8(a) Frequency dependent real part of Impedance (Z') for BST ceramics. (b) Frequency dependent Imaginary part of Impedance (Z") for BST ceramics.

Impedance (Nyquist) analysis of $Ba_{0.8}Sr_{0.2}TiO_3$ ceramics are shown in Figure 9. The Nyquist plots of the $Ba_{0.8}Sr_{0.2}TiO_3$ ceramics exhibit a single broad depressed semicircular response over the investigated frequency range, indicating a dominant non-Debye relaxation process. Since no distinct second arc attributable independently to grain and grain boundary responses could be resolved, a simplified R ‖ CPE equivalent circuit was employed. The CPE was introduced to account for the depressed nature of semicircle and distribution of relaxation times arising from microstructural heterogeneity. The impedance of CPE is expressed as $Z_{CPE} = [Q(jw)^n]^{-1}$, where Q is CPE coefficient and n is CPE exponent. The fitted n values fall within the physically meaningful range $0<n<1$, confirming non-ideal capacitive behaviour [27-28]. The resulting fitting parameters are summarized in Table 4. The effective relaxation resistance varies non monotonically with sintering temperature, indicating that electrical response is governed by the competing effects of densification, grain growth, defect redistribution and changes in the microstructural relaxation environment. The CPE exponent (n) values lie between 0.87 and 0.92, confirming non ideal capacitive relaxation with distribution times. The absence of systematic monotonic variation in n suggests that the degree of electrical heterogeneity is not controlled solely by sintering temperature. Similar results have been reported in the literature [29].

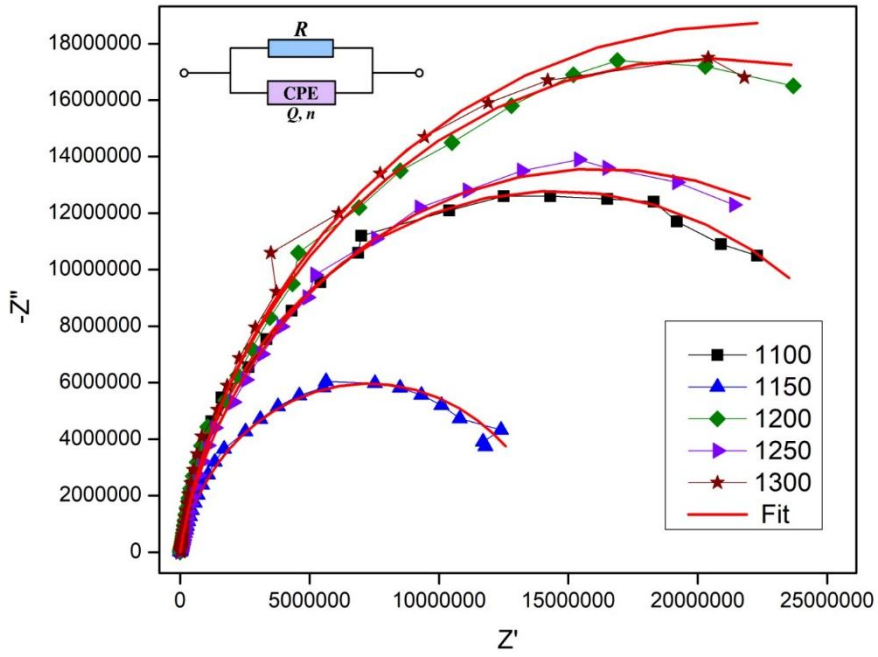

Figure 9. Cole-Cole plots of BST ceramics

Table 4. Equivalent circuit fitting parameters obtained from impedance spectroscopy for $B_{0.8}S_{0.2}TiO_3$ ceramics sintered at different temperatures.

Ceramic Sample	R(Ω)	Q(S s^n)	n	C_{eff}(F)	τ(s)	f_{max}(Hz)
BST1100	$2.901x10^7$	$4.078\ x10^{-11}$	0.919	$2.250\ x10^{-11}$	$6.527\ x10^{-4}$	243.8
BST1150	$1.452\ x10^7$	$8.028\ x10^{-11}$	0.874	$3.020\ x10^{-11}$	$4.384\ x10^{-4}$	363.1
BST1200	$4.121\ x10^7$	$6.411\ x10^{-11}$	0.896	$3.210\ x10^{-11}$	$1.323\ x10^{-3}$	120.3
BST1250	$3.233\ x10^7$	$6.487\ x10^{-11}$	0.889	$2.994\ x10^{-11}$	$9.677\ x10^{-4}$	164.5
BST1300	$4.429\ x10^7$	$7.422\ x10^{-11}$	0.889	$3.641\ x10^{-11}$	$1.613\ x10^{-3}$	98.7

Frequency dependence of AC conductivity indicates a low frequency region in which the conductivity is comparatively weakly frequency dependent, followed by a dispersive high frequency region. The low frequency response can be associated with the restricted motion of charge carriers by resistive grain boundary regions, whereas the high frequency dispersion is consistent with localized or hopping type charge transport. The systematic variation with sintering temperature suggests that microstructural evolution, particularly grian growth and changes in grain boundary connectivity, influences the measured electrical transport. Although defect mediated hopping may contribute to the observed response, assignment to a specific defect species such as oxygen vacancies requires complementary defect sensitive measurements and is therefore not made conclusively here.

The combined structural, microstructural and electrical results demonstrate that the sintering temperature acts a as a key processing variable controlling the electrical response of $Ba_{0.8}Sr_{0.2}TiO_3$

ceramics. Increasing the sintering temperature reduces diffraction peak broadening and promotes crystalline coarsening, while FESEM observations reveal substantial grain growth and progressive reduction of residual porosity. These microstructural changes modify the relative volume fraction and electrical contribution grain interiors and grain boundary regions. The dielectric response cannot be considered independently of the microstructure. The increase in grain size and reduction in porosity decrease the relative contribution of low permittivity regions, whereas changes in grain boundary density and resistance modify dielectric relaxation and AC charge transport. The impedance response provides complementary evidence for this evolution through the temperature dependent changes in resistive and capacitive contributions of the ceramic. Consequently, the observed dielectric and conductivity trends originate from the coupled evolution of crystallinity, grain size, porosity and grain boundary electrical response rather than from sintering temperature alone. These results establish a processing-microstructure-electrical property relationship in which sintering temperature controls the microstructural state of BST and latter governs the relative contributions of dielectric polarization, relaxation and charge transport.

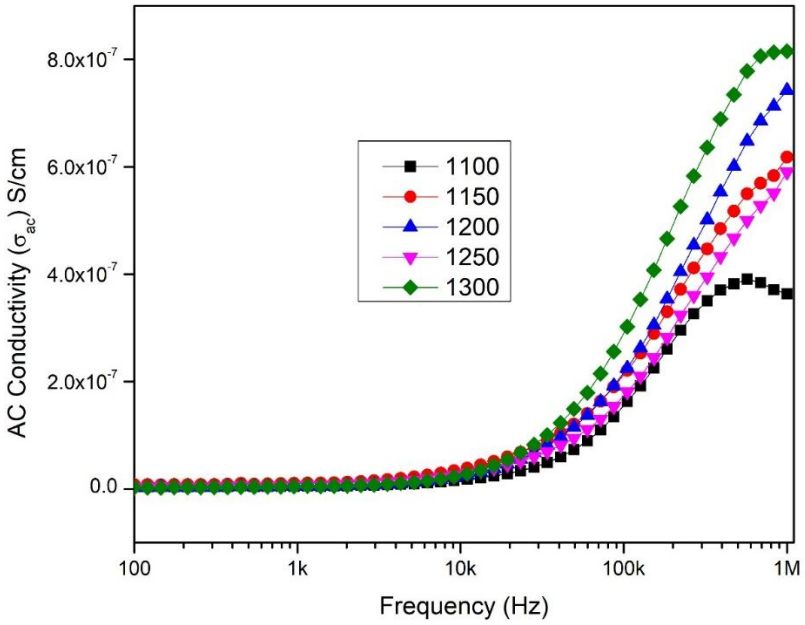

Figure 10. AC conductivity of BST Ceramics sintered at different temperatures.

4.Conclusions

The solid-state reaction technique was utilized to synthesize BST ceramics and examine the role of sintering temperature on their structural, microstructural, and dielectric properties. XRD analysis revealed diffraction patterns consistent with the perovskite phase, with no secondary crystalline phases detected within the sensitivity of the measurements. The principal diffraction peak FWHM decreased from 0.298º to 0.104º with the rise in sintering temperature. FESEM and quantitative image analysis revealed substantial grain growth, with the average grain size increasing from 0.43 μm to 4.15 μm. The dielectric measurements showed an increase in the maximum

dielectric constant and a reduction in dielectric loss with increasing sintering temperature, while the dielectric maximum remained near 80 ºC. Modified Curie-Weiss analysis of BST1300 sample yielded a diffuseness exponent of approximately 1.41, consistent with diffuse dielectric transition. Impedance spectra exhibited non-ideal relaxation behaviour that could be represented usings a simplified resistor-CPE equivalent circuit. The AC conductivity measurements further demonstrated frequency dependent electrical transport. Overall, The findings establish a relationship between sintering induced microstructural evolution and dielectric and electrical response of BST ceramics. The results also highlight the need to distinguish FESEM grain size from XRD derived crystallite size and to interpret equivalent circuit parameters within the limitations of the selected model. This integrated characterization provides a basis for understanding and optimizing the processing conditions of BST ceramics for dielectric applications.

Funding Declaration
No funding was received for this research.

References

1. Huiling Du, Cuiying Ma, Wuxiang Ma, Haiting Wang, Microstructure evolution and dielectric properties of Ce-doped $SrBi_4Ti_4O_{15}$ ceramics synthesized via glycinenitrate process, Process. Appl. Ceram. 12 (4) (2018) 303–312, https://doi.org/ 10.2298/PAC1804303D.
2. Anuradha Kumari, Barnali Dasgupta Ghosh, Effect of strontium doping on structural and dielectric behaviour of barium titanate nanoceramics, Adv. Appl. Ceram. 117 (7) (2018) 427–435, https://doi.org/10.1080/ 17436753.2018.1491166.
3. N. Sareecha, W.A. Shah, M.L. Mirza, A. Maqsood, M.S. Awan, Electrical investigations of Bi-doped $BaTiO_3$ ceramics as a function of temperature, Physica B 530 (2018) 283–289, https://doi.org/10.1016/j.physb.2017.11.069.
4. Ming-li Li, Hui Liang, Ming-xia Xu, Simple oxalate precursor route for the preparation of brain-like shaped barium–strontium titanate: $Ba_{0.6}Sr_{0.4}TiO_3$, Mater. Chem. Phys. 112 (2) (2008) 337–341, https://doi.org/10.1016/j. matchemphys.2008.06.016.
5. Xiao Wei, Gang Xu, Zhaohui Ren, Yonggang Wang, Ge Shen, Gaorong Han, Composition and shape control of single-crystalline $Ba_{1-x}Sr_xTiO_3$ (x=0–1) nanocrystals via a solvothermal route, J. Cryst. Growth 310 (18) (2008) 4132–4137, https://doi.org/10.1016/j.jcrysgro.2008.04.039.
6. Haitao Huang, James F. Scott (Eds.), Ferroelectric Materials for Energy Applications, John Wiley & Sons, 2018.
7. Venkata Ramana Mudinepalli, Leng Feng, Wen-Chin Lin, B. S. Murthy, Effect of grain size on dielectric and ferroelectric properties of nanostructured $Ba_{0.8}Sr_{0.2}TiO_3$ ceramics, Journal of Advanced Ceramics 2015, 4(1): 46–53, DOI: 10.1007/s40145-015-0130-8
8. Jakkula shankar, A. Shiva Kumar, P. Raju , S. Rajesham , S.K. Mahammad Ali, Physical and microstructural properties of $Ba_{1-x}Sr_xTiO_3$ ceramics with heat treatment, Ceramics International 51 (2025) 6506–6514, https://doi.org/10.1016/j.ceramint.2024.12.094

9. Jan Suchanicz et al, Temperature and E poling evolution on structural, vibrational,dielectric and ferroelectric properties of $Ba_{1-x}Sr_xTiO3$ ceramics (x= 0,0,1,0,2,0,3,0.4 and 0.45), Materials (2023), 16, 6316. https://doi.org/10.3390/ma16186316
10. Jeon, J.-H. Effect of SrTiO3 concentration and sintering temperature on microstructure and dielectric constant of $Ba_{1-x}Sr_xTiO_3$, J. Eur. Ceram. Soc. 2004, 24, 1045–1048. https://doi.org/10.1016/S0955-2219(03)00385-6
11. Dependence of the structural and dielectric properties of $Ba_{1-x}Sr_xTiO_3$ ceramic solid solutions on raw material processing,J. Eur. Ceram. Soc., 19 (1999), pp. 2015-2020, https://doi.org/10.1016/S0955-2219(99)00010-2
12. A Shiva Kumar, R. V. Sudheer Kumar, S. K. Mahammad Ali, Materials Today: Proceedings 92 (2023)1070–1073, https://doi.org/10.1016/j.matpr.2023.05.075.
13. R.E. Pătru, C.A. Stanciu, V.A. Surdu, E.M. Soare, R.D. Truşcă, B.S. Vasile, A.I. Nicoară, L. Trupină, I. Pasuk, M. Botea, N. Horchidan, L. Mitoşeriu, L. Pintilie, I. Pintilie, A.C. Ianculescu, Downscaling grain size toward the nanometre range – A key-factor for tuning the crystalline structure, phase transitions, dielectric and ferroelectric behaviour in $Ba_{0·8}Sr_{0·2}TiO_3$ ceramics, Progress in Solid State Chemistry,74 (2024), 100457. https://doi.org/10.1016/j.progsolidstchem.2024.100457.
14. J. Ćirković et al. Dielectric and ferroelectric properties of BST ceramics obtained by a hydrothermally assisted complex polymerization method, Ceramics International 41 (2015) 11306–11313, https://doi.org/10.1016/j.ceramint.2015.05.088.
15. Shaista Yousuf and Mohd Ikram. Unveiling the structural and optical characteristics of $Ba_{0.8}Sr_{0.2}TiO_3$-$NiFe_2O_4$ composites, Ceramics International,51 (2025).64403-64415, https://doi.org/10.1016/j.ceramint.2025.11.176
16. Feng Jiang, Entao Zheng, Guo Feng, Qing Yang, Wenwei Jin, Chuan Shao, Jianmin Liu, Dahai Wang, Jian Liang, Effects of different processing parameters on structure of $Ba_{1-x}Sr_xTiO_3$ powders synthesized via nonhydrolytic sol-gel method. Processing and Application of Ceramics. 18 (2024). 224-233. https://doi.org/10.2298/PAC2402224J
17. Mohammed Mesrar, Laila Mesrar, Taj-dine Lamcharfi, Abdelhalim Elbasset Farid Abdi , Nor-Said Echatoui, Lha El Hachemi Omari, Multifunctional properties of Mg-doped $(Ba_{0.85}Sr_{0.15})TiO_3$ ceramics: A combined structural, dielectric, electromechanical, and impedance analysis, Chemical Physics Impact. 11 (2025) 100895 https://doi.org/10.1016/j.chphi.2025.100895.
18. Preeti Saroha , Anshu Gaur, Meenal Dhanetwal , Md Ahamad Mohiddon, Structural, dielectric, ferroelectric and electrocaloric properties of Y–Li Co-doped $Ba_{0.8}Sr_{0.2}TiO_3$ ceramics, Journal of Physics and Chemistry of Solids 218 (2026) 113862, https://doi.org/10.1016/j.jpcs.2026.113862
19. Shaista Yousuf and Mohd Ikram, Insights into electric, magnetic, and magneto-electric properties of (1-x) $Ba_{0.8}Sr_{0.2}TiO_3$-(x)$NiFe_2O_4$ multiferroic composites: Relaxation dynamics and energy storage applications, Ceramics International 51 (2025) 23499–23519, https://doi.org/10.1016/j.ceramint.2025.03.039

20. Yina Zheng, Guo Feng, Chao Chen, Feng Jiang, Chong Zhao, Qian Yuan, Lingxian Sun, Na Tu, Yunjing Chen, Xiangping Jiang, Improved piezo-photocatalysis performance of $Ba_{1-x}Sr_xTiO_3$ nano-podwers via synergistically optimizing phase ratio, defects and polarization, Journal of Alloys and Compounds 1011 (2025) 178348, https://doi.org/10.1016/j.jallcom.2024.178348
21. Xu Q, Zhang X-F, Liu H-X, et al. Effect of sintering temperature on dielectric properties of $Ba_{0.6}Sr_{0.4}TiO_3$-MgO composite ceramics prepared from fine constituent powders. Mater Design 2011, 32: 1200–1204.
22. Shaw TM, Trolier-McKinstry S, McIntrye PC. The properties of ferroelectric films at small dimensions. Annu Rev Mater Sci 2000, 30: 263–298. Xiaoyu Wu, Wei Li, Ziheng Huang, Weitian Wang,
23. Effect of sintering temperature on the dielectric and impedance properties of high-entropy perovskite oxides (Bi0.2La0.2Ba0.2Sr0.2Ca0.2)TiO3, Materialia, Volume 45,2026,102644.https://doi.org/10.1016/j.mtla.2025.102644.
24. K. Uchino, S. Nomura, Critical exponents of the dielectric constants in diffused phase-transition crystals, Ferroelectrics 44 (1982) 55–61, https://doi.org/10.1080/00150198208
25. Muhammad Arshad, Du Huiling,, Javed Muhammad Sufyan, Asghari Maqsood, Iqra Ashraf, Shahid Hussain, Wanli Ma, Hongpei Ran, Fabrication, structure, and frequency-dependent electrical and dielectric properties of Sr-doped $BaTiO_3$ ceramics, Ceramics International 46 (2020) 2238–2246, https://doi.org/10.1016/j.ceramint.2019.09.208
26. Driss Akhlidej, Abdelhalim Elbasset, Farid Abdi, Nor-Said Echatoui, Lhaj El Hachemi Omari, Microstructural control of BaTiO3 ceramics: Influence of sintering temperature induced microstructural evolution on electrical and dielectric behavior, Ceramics International,2026, https://doi.org/10.1016/j.ceramint.2026.07.474.
27. C.M.A. Brett, Electrochemical impedance spectroscopy in the characterisation and application of modified electrodes for electrochemical sensors and biosensors, Molecules 27 (5) (Feb. 2022) 1497, https://doi.org/10.3390/molecules27051497.
28. Joshi, S., Shukla, A. Structural, electrical, and optical characterization of Sm-Doped BiFeO3 ceramics synthesized via sol-gel method. J Electroceram (2026). https://doi.org/10.1007/s10832-026-00479-4
29. Vidushi Karol, , Parveen Kumar , Renu Rani, Ankurava Sinha , Prianka Sharma, Chandra Prakash, Anshu Awasthi, Structural transformation and impedance characterization of Mg-doped $Ba_{0.95}$-$xMg_xSr_{0.05}TiO_3$ ceramics: Evidence of compositional tuning in activation energy and relaxation behavior, Ceramics International 52 (2026) 1335–1344. https://doi.org/10.1016/j.ceramint.2025.11.374